



HAL
open science

CFD Application to Gun Muzzle Blast -A Validation Case Study

Daniel L Cler, Nicolas Chevaugéon, Mark S Shephard, Joseph E Flaherty

► **To cite this version:**

Daniel L Cler, Nicolas Chevaugéon, Mark S Shephard, Joseph E Flaherty. CFD Application to Gun Muzzle Blast -A Validation Case Study. 41st AIAA Aerospace Science Meeting and Exhibit, AIAA, Jan 2003, Reno, Nevada, USA, United States. 10.2514/6.2003-1142 . hal-03939856

HAL Id: hal-03939856

<https://hal.science/hal-03939856>

Submitted on 15 Jan 2023

HAL is a multi-disciplinary open access archive for the deposit and dissemination of scientific research documents, whether they are published or not. The documents may come from teaching and research institutions in France or abroad, or from public or private research centers.

L'archive ouverte pluridisciplinaire **HAL**, est destinée au dépôt et à la diffusion de documents scientifiques de niveau recherche, publiés ou non, émanant des établissements d'enseignement et de recherche français ou étrangers, des laboratoires publics ou privés.

CFD Application to Gun Muzzle Blast – A Validation Case Study

by

Daniel L. Cler^{*}

*Benet Laboratories – TACOM/ARDEC – U. S. Army
Watervliet, NY*

Nicolas Chevaugon,[†] *Mark S. Shephard*,[‡]
and Joseph E. Flaherty^{††}

*Rensselaer Polytechnic Institute,
Troy, NY*

Jean-Francois Remacle^{‡‡}

*Université Catholique de Louvain
Louvain-la-Neuve, Belgium*

*41st AIAA Aerospace Sciences Meeting and Exhibit
Reno, Nevada
January 6-9, 2003*

Abstract

Accurate modeling of near-field wave propagation is critical to determine blast wave overpressure of large caliber muzzle brakes. Experimental testing to determine blast overpressure is costly, making CFD (Computational Fluid Dynamics) simulations of these flow-fields a viable alternative. Techniques and specialized CFD codes are being developed in order to properly model the unsteady, very high-pressure flows of gun muzzle blast.¹⁻⁴

Two CFD codes, Fluent 6.1.11 (a pre-release version of Fluent) and

the Discontinuous Galerkin Code (DG), developed at Rensselaer Polytechnic Institute⁵ were used in a comparison to experimental shadowgraph data from the 7.62 mm NATO rifle G3 using a DM-41 training round for the purpose of developing CFD modeling techniques and validation of the CFD codes. Unsteady grid adaption was used with both solvers in order to reduce solution error near unsteady blast waves and shocks. It is possible to get good results from Fluent with high levels of adaption, however DG, can model blast with courser grid adaption. It was also found that DG required an order of magnitude longer solution time than Fluent for a given number of grid elements. The 7.62 mm NATO G3 CFD precursor flow results matched experimental shadowgraph results well, however, the main propellant flow did not.

^{*}Mechanical Engineer

[†]Post-Doctoral Research Associate, Scientific Computation Research Center

[‡]Johnson Professor of Engineering, Associate Fellow AIAA

^{††}Amos Eaton Professor of Computer Science

^{‡‡}Assistant Professor of Civil Engineering

This material is declared a work of the U.S. Government and is not subject to copyright protection in the United States.

Introduction

Tank cannon muzzle brakes are becoming a critical technology for future combat systems as recoil loads increase and system weight decreases. Muzzle brakes redirect forward momentum of the muzzle gases rearward to offset recoil load created by the cannon during firing. A deleterious effect of redirecting the muzzle gases rearward is high-pressure waves behind the cannon where operational personnel are located. Limitations are placed on blast overpressure because of physiological reasons, both to the body and ear of nearby troops. Experimental, full-scale testing of tank cannon systems is very expensive. As a result, simulation of the muzzle brake flow field is highly desirable as an early design tool.

Developing the specific techniques to model blast wave propagation of high pressure, high-temperature gun propellant gases is critical to correctly simulating blast overpressure. In order to do this, a validation case with sufficient quantitative and qualitative information about the very complex flow-field created by muzzle blast is necessary in order to properly validate CFD techniques. A CFD analysis of the 7.62 mm NATO rifle G3 with a DM-41 round was selected because of the large quantity of public domain information about the flow-field in the form of shadowgraph images and analysis.¹

Symbols

CFD	Computational Fluid Dynamics
CFL	Courant-Friedrichs-Levy criterion
C_p	specific heat at constant

DG	Pressure, N-m/kg-°K Discontinuous Galerkin Code
DGM	Discontinuous Galerkin Method
p	static pressure, MPa
p_e	gun muzzle exit pressure
p_∞	free stream ambient pressure
R	gas constant, N-m/kg-°K
γ	ratio of specific heats
t	CFD flow time, sec
t_{exp}	experimental flow time, sec or μ sec
T	static temperature, °K
V	velocity, m/s
ρ	density, kg/m ³

Problem Description

The blowdown or emptying of a gun barrel after the projectile leaves the barrel is similar to the free jet expansion process. Because of the high pressures typically seen in guns, pressure ratios range from 5 to 1000. As a result, the flow exiting the barrel is typical of highly under-expanded jet flow. The flow-field around the muzzle of a gun barrel can be complicated and include flow phenomena such as expansion waves, compression waves, shocks, shear layers, and blast waves at speeds up to Mach 7 to 10 (see Figure 1).

As the flow exits the barrel at the muzzle and begins to expand around the sharp corner of the gun barrel, a Prandtl-Meyer expansion fan forms at the muzzle plane and spreads angularly away from the gun axis and then terminates at the free-shear jet-boundary or contact surface of the muzzle flow. These expansion waves reflect off the jet boundary forming a series of weak compression waves that coalesce to form a barrel or intercepting

shock. In addition, these waves can propagate into the flow field toward the main blast wave.¹

Downstream of the muzzle, a Mach disk forms across which the flow decelerates from supersonic to subsonic velocities. The Mach disk and barrel shock enclose a volume known as the shock-bottle. Initially the Mach disk is constrained by a blast-wave front or primary shock moving at sonic speed. This constraining action can be seen as a deformation in the plume boundary.¹

Outside of the barrel shock, at the corners of the Mach disk a turbulent vortex ring forms as the flow tries to move toward the blast wave, but is constrained. The outside edge of this turbulent vortex ring forms the plume boundary. The turbulent vortex ring is caused by the large difference in tangential velocity and turbulent shear layer near the jet boundary. Once the blast moves away from the muzzle, the flow from the muzzle is similar to an unrestrained free jet expansion. At this point, the flow from the muzzle is similar to that exiting a rocket exhaust nozzle.¹

The problem selected for validation this CFD validation is the 7.62mm NATO G3 rifle with a 400 mm barrel length shooting a standard DM41 training round. This particular configuration has a blow down characterized by two precursor shocks and the main propellant flow.

A precursor shock is formed as the bullet begins to accelerate down the barrel causing compression waves to be formed in front of the bullet as the air column in front of the bullet accelerates. In

addition, leakage of propellant gases past the bullet can cause the air column to accelerate as well. The compression waves caused by the acceleration of the air column coalesce to form a “precursor” shock. Depending on the speed of the bullet and the length of time the bullet is in the barrel, a second precursor shock may form. The precursor flow emanating from the muzzle is easily visualized with shadowgraph because the gas column contains mostly air as opposed to cloudy propellant gas. For this reason, it is easier to compare to CFD results. The pressure ratios for the two precursor shocks for the 7.62mm NATO G3 are 6 for the first precursor and 15 for the second precursor.

After the bullet exits from the barrel and uncorks the propellant gas column behind it, the flow of the main propellant gases begins. The main propellant flow is similar to the precursor flow, only with pressure ratio typically one to two orders of magnitude higher. The precursor contributes very little to the overall blast effect of the gun. The propellant gas exits the barrel at a pressure ratio of 660. Because the pressure is so much higher than the precursor wave, the main blast wave quickly overtakes the precursor blast wave. In addition, because of the large quantities of unburnt propellant and water vapor in the propellant gases, viewing the shock structure of the main propellant blast wave with shadowgraph is very difficult.

Discontinuous Galerkin Code Background

The Discontinuous Galerkin Method (DGM) was introduced by Reed and Hill

in 1973.⁶ Recently the method has become popular in solving fluid dynamic problems. The DGM is somewhere between a finite element and finite volume method. DGM allows double discretization or discretization of the geometrical computational domain (the grid) as well as the functional domain (flow equations). This allows one to adapt both the grid elements and the order of the flow equations. Adaption of the grid is typically referred to as h-refinement and adaption of the flow equations to different orders as p-refinement. Both refinement techniques combined can optimize the computational effort required for complex blast analysis problems.⁵

DGM also allows for more general mesh configurations such as non-conformal meshes and discontinuous functions at the edge of the elements. This greatly simplifies both h-refinement and p-refinement. The main advantage of being able to solve discontinuous functions when analyzing shock dependent problems is that shock structures and shock sharpness can still be maintained, even with very low levels of h-refinement or grid adaption. This is not true with continuous based solvers. H-refinement and p-refinement was performed using density as an error indicator.⁵

In addition to being able to perform h-refinement and p-refinement, DGM also can perform local time stepping while using an explicit inviscid solver with explicit time-stepping to perform unsteady flow calculations such as blast. Local time stepping is a means by which a local CFL criteria is applied to each cell and then that and similar sized cells are solved at that CFL number. For

example, if one full-sized cell in the domain and one-half-sized cell in the domain have similar flow properties, then the CFL limited explicit time step size should be one-half as large for the one-half-sized cell. In this instance, two iterations would be performed on the half-sized cell, while only one iteration would be performed on the full-sized cell with local time-stepping. This could then be extended to the entire computational space and thereby reduce the total number of iterations required. This method also allows one to set the flow time step size, unlike typical explicit solver. Explicit time step flow solvers tend to be more efficient and time accurate for solving blast wave problems than implicit schemes. A shock limiter is used to limit pressure gradients near shocks to physical levels. These techniques have been incorporated into a CFD solver, referred to as DG, being developed by the Scientific Computation Research Center, Rensselaer Polytechnic Institute.

Fluent Background

Fluent is a commercial CFD code that can perform solutions on various kinds of fluid dynamic problems. Recently, Fluent developed the capability to perform unsteady grid adaption (h-refinement) in a soon to be released version of the code, Fluent 6.1. A prerelease version of the code was used on the 7.62mm NATO G3 problem in order to validate the unsteady grid adaption capability. The unsteady grid adaption capability within Fluent can perform non-conformal grid adaption. For this analysis, adaption was performed using density gradient as an error estimator. Solution refinement was limited by specifying a minimum cell

size of $2.5e-8 \text{ m}^2$. This resulted in refinement levels of up to six for the analysis of the first precursor flow. The second order inviscid solver was used to solve the explicit flow equations with an explicit time stepping scheme.

CFD Setup and Boundary Conditions

The 7.62mm NATO G3 rifle with a 400 mm barrel length shooting a standard DM 41 training round was modeled using a 2-D half-grid tri-mesh and 2-D half-grid quad-mesh shown in Figures 2 and 3 respectively. The grid was made using Gambit, a meshing tool produced by Fluent, Inc.

The modeling of blast problems utilizing 2-D rather than axisymmetric boundary conditions presents a problem. Blast wave development is inherently a three-dimensional problem. Blast wave strength appears to be much higher than it actually is when utilizing 2-D boundary conditions. This effect is accentuated the further the blast wave is from the muzzle or source. The results presented in this paper are limited to 2-D because of a limitation in the DG solver to only run 2-D simulations and not axisymmetric.

A time varying pressure inlet was used to control total pressure, static pressure, static temperature, and mass fraction of the air and K503 propellant (only Fluent modeled the change from air to K503, DG utilized air for all flows) at 12.5 mm upstream of the muzzle (see Figures 2 and 3). The experimental data used for the pressure inlet boundary condition is based upon the measured static muzzle pressure of the NATO rifle shown in Figure 4 below. Modifications to the release times of the second precursor and

main propellant were required to match shadowgraph results. The K503 propellant characteristics along with the static pressure data were then used to derive the other required parameters for the pressure inlet using unsteady compressible flow theory. Because of the lack of information about the initial boundary conditions, it is possible that computation errors could occur in the CFD results. The boundary conditions are defined in CFD flow time, t , where time $t = 0.0$ corresponds to the flow beginning 12.5 mm upstream of the muzzle for the first precursor. This time, $t = 0.0$, would correspond to a flow time from the experiment of $t_{\text{exp}} = -400 \text{ } \mu\text{sec}$. The boundary conditions used for the unsteady pressure inlet are as follows:

Gas Properties:

Air:

$$R = 287 \text{ N}\cdot\text{m}/\text{kg}\cdot\text{K}$$

$$\gamma = 1.4$$

$$C_p = 1006 \text{ N}\cdot\text{m}/\text{kg}\cdot\text{K}$$

K503 (used for Fluent analysis only):

$$\gamma = 1.3$$

$$C_p = 2000 \text{ N}\cdot\text{m}/\text{kg}\cdot\text{K}$$

Initial Conditions:

$$p = 101325 \text{ Pa}$$

$$V = 0.0 \text{ m/s}$$

$$T = 300 \text{ }^\circ\text{K}$$

$$\rho = p/RT$$

Precursor 1:

$$@ t < 342.28 \text{ } \mu\text{sec}$$

$$p = 0.6 \text{ MPa}$$

$$V = 548.1 \text{ m/s}$$

$$T = 631.626 \text{ }^\circ\text{K}$$

$$\rho = p/RT$$

Precursor 2:

@ 342.28 < t < 399.2 μsec

$$\begin{aligned}p &= 1.5 \text{ MPa} \\V &= 905.146 \text{ m/s} \\T &= 838.8 \text{ }^\circ\text{K} \\ \rho &= p/RT\end{aligned}$$

Main Propellant Flow:

@ t > 399.2 μsec

$$\begin{aligned}p &= 101325 * 659.369 e^{(-1.484.8 * (t - 0.0004015))} \text{ MPa} \\V &= 905.146 \text{ m/s} \\T &= 1700 \text{ }^\circ\text{K} \\ \rho &= p/RT\end{aligned}$$

It should be noted that the starting times for the second precursor and main propellant flows had to be adjusted relative to the starting times shown in Figure 4. This was necessary to get the CFD results to match the shadowgraph images properly. The inaccuracy in start time of these events is possibly because of inaccuracies in measurement times of the pressure at the 12.5 mm or because of improper specification of boundary conditions for the CFD problem. The exponential pressure equation for the main propellant flow shown above was not modified for the new main propellant start time.

The solution was run using the unsteady explicit solver with explicit local time stepping. However, the local time step cannot be larger than 10-20 times as large as the minimum cell size CFL criterion. The CFL limit for each cell was limited to 0.3 to allow for curvature in flow properties within each cell to be resolved. The material properties of the species were modeled including the specific heat at constant pressure and gas constant.

A constant pressure, velocity, and density far-field boundary condition with values identical to the initial conditions was utilized. The far-field boundary is approximately 100 calibers from the muzzle with most of the flowfield phenomena being investigated occurring within 25 calibers of the muzzle.

Muzzle blast typically consists of over-expanded nozzle flow interacting with blast wave shocks. To model these propagating shocks well, it is necessary to have fine grid near the shock front as it passes through the flow domain. To minimize solution time, non-conformal grid adaptation is utilized to adapt to density gradients. Various levels of adaption were investigated. For the solutions, various grid types and h-refinement levels were used including a DG tri-mesh grid at 5-levels of adaption for solution times up to $t_{\text{exp}} = -250 \text{ } \mu\text{sec}$, an adapted DG quad-mesh grid at 4-levels of adaption for solution times past $t_{\text{exp}} = -250 \text{ } \mu\text{sec}$, and a Fluent tri-mesh grid at $2.5e-8\text{m}^2$ minimum cell size adaption level. Each of these grid types are shown in Figure 5 at $t = 1.0e-4$ seconds. The mesh adaption was performed every other time step for both the DG and Fluent analyses. The time step for the Fluent analysis was dictated by the CFL = 0.5 criterion applied to the smallest cell in the flow domain. The time step for DG 5-level tri-mesh was based on a local time step setting of $2.0e-7$ seconds for the 5-level tri-mesh and $5.0e-7$ seconds for the 4-level quad-mesh.

For this particular study, only non-conformal h-refinement of the grid was performed for the DG code. P-refinement was not used for the DG simulations and the polynomial order of

the flow equations was fixed at first order. For the Fluent simulations, the flow equations were fixed second order.

Results

The first precursor shock is created in the muzzle by the compression of the air in the gun tube by the accelerating bullet. This shock wave exits the barrel at approximately $t_{\text{exp}} = -400 \mu\text{s}$ before shot exit. Figures 6-16 present comparisons of shadowgraphs of experimental data³ and logarithmic density grayscale contour plots from 395 microseconds as the first precursor begins to exit the barrel until 120 microseconds after the main propellant flow begins.

In the comparison figures, a logarithmic density grayscale contour plot of the CFD results was used to compare to experimental shadowgraph images. Shadowgraph shows curvature of density throughout the flow field. By using a logarithmic scale for the CFD density contours, weak shock patterns such as the primary blast wave are more visible and easier to compare to experimental shadowgraph images.

It should be noted that in some of the shadowgraph images a 50mm ruler is placed on the barrel to provide a reference measurement. In addition, a collar on the end of the barrel is present. The ruler and collar were not modeled in the CFD simulation.

As can be seen in Figure 6 at $t_{\text{exp}} = -395 \mu\text{s}$, the exit of the first precursor shock wave is about the same distance from the gun tube with a similar thickness and shape for the DG simulation. In addition, the DG simulation shows the

beginning of the vortical flow at the corners of the muzzle. This corner flow is not as visible in the shadowgraph image. This corner flow later develops into an expansion wave.

In Figure 7 at $t_{\text{exp}} = -370 \mu\text{s}$, the outer spherical shock of the first precursor has developed. The outer blast wave has a nearly identical shape and size for both the Fluent and DG simulations. In addition, the Mach disk is modeled, but is a slightly different shape than the experimental data. The barrel shock and free-shear layer are both modeled with the CFD simulation, however the free-shear layer has a greater angle relative to the barrel and the barrel shock a lower angle. The barrel shock is just barely visible in the shadowgraph image. The outer free-shear layer is more visible in the shadowgraph image. In addition, the vortex ring is beginning to form showing a similar shape and size as the shadowgraph for both the Fluent and DG results. In the DG results, the free-shear layer shows disturbances propagating from the muzzle corner that are not present in the Fluent results or seen in the shadowgraph. This could be due to the discontinuous nature of the DG code to determine acoustic propagations.

In Figure 8 at $t_{\text{exp}} = -350 \mu\text{s}$, the shock bottle has now formed as seen in the shadowgraph as formed by the edges of the barrel shock and the downstream Mach disk. In addition, more complex shock interactions occur. The beginning of the vortex at the corner of the shock bottle is beginning to form. The vortex formation is seen in both the DG and Fluent results. The DG results show more turbulence than the Fluent results. In addition, the waves propagating from the corner of the muzzle are more

pronounced with DG. The inner barrel shock is visible in both DG and Fluent results. The outer blast wave is about the same size and distance from the muzzle with both DG and Fluent. The DG results also show waves propagating toward the rear edge of the blast wave. These waves are the result of the vortex formation. The plume boundary is also visible in the DG and Fluent results shown by a change from dark to light at the front of the Mach disk.

In Figure 9 at $t_{\text{exp}} = -250 \mu\text{s}$, the jet flow is fully developed and the typical shock diamond pattern of an over-expanded jet now exists as shown in the shadowgraph. The over-expanded jet flow occurs because the outer shock boundary has propagated far enough from the main jet that the muzzle flow expansion is uninhibited. The vortex flow at the corner of the Mach disk and free-shear layer is still present in the CFD images. The free-shear layer has a slightly higher angle in the CFD results and the barrel shock is not as sharp. Fluent shows the oblique shocks emanating downstream of the Mach disk more clearly than DG, however both codes smear these shocks substantially. The plume boundary is visible with both codes. Once again, the waves propagating from the corner of the muzzle barrel are seen with DG and not with Fluent. In addition, DG shows waves propagating toward the rear blast wave. These waves can also be seen in the shadowgraph.

In Figure 10 at $t_{\text{exp}} = -80 \mu\text{s}$, the flow is more developed. For the rest of the results there are no Fluent comparisons and a 4-level quad-grid was used for the DG solution. A coarser initial grid and a lower level of refinement were used for

the longer solution times due to the high CPU time required for these simulations. DG shows substantially more shock structure. The oblique shocks emanating from the corner of the Mach disk not visible at $t_{\text{exp}} = -250 \mu\text{s}$ are now clearly visible. Either these shocks are delayed or they are obscured in the shadowgraph image by the high level of turbulence. The free-shear layer is also at a higher angle once again with the DG results. In addition, there is less turbulent structure in the DG results because of running an inviscid solution without a turbulence model, however most of the large-scale turbulence is still present. The plume appears to be less elongated for DG. DG also shows the blast waves emanating from the turbulent vortices that are not shown in the shadowgraph. The main blast wave for DG appears to be similar in shape to the shadowgraph, but possibly farther downstream from the gun tube. The waves propagating from the gun tube corner are smeared more due to the lower level of grid resolution.

In Figure 11 at $t_{\text{exp}} = -40 \mu\text{s}$, the second precursor shock is shown. The rear blast wave in the second precursor from the DG solution is similar to the shadowgraph image. The front of the precursor shows a shock wave in the DG solution, that is not present in the shadowgraph. The first precursor plume is also slightly larger. The Mach disk from the first precursor is visible in the DG solution as well as the oblique shocks emanating from the corner. These shocks can be seen inside the plume turbulence in the shadowgraph.

In Figure 12 at $t_{\text{exp}} = -5 \mu\text{s}$, the flow main blast wave has begun to exit the gun barrel. Once again, the front of the main blast wave is much wider than the

shadowgraph as was the case for the second precursor. The second precursor has a similar shape and size as the shadowgraph, with the exception being the front of the precursor wave. The presence of the first precursor seems to have a strong effect on the second precursor in the DG results. It appears that there is more dissipation in the shadowgraph. This in part could be a result of the presence of significant turbulence. This turbulence is breaking up the shock structure. This breakup is not occurring with the DG results. This indicates the need for some turbulence modeling in the CFD.

In Figure 13 at $t_{\text{exp}} = +35 \mu\text{s}$, the main blast wave flow is shown. Once again, turbulence has smeared a lot of the shock structure in the shadowgraph that is present in the DG results. In addition, the basic shape of the blast wave is distorted, both at the rear, but especially at the front. The shock angle for the free shear layer is at a very high angle compared to the precursor flow. The angle is similar in both the shadowgraph and DG results. The core muzzle flow is shown as a dark spot on the shadowgraph and a light spot for the DG results. The barrel shock angle indicated by the edge of the bright area in the DG results and a sharp dark edge inside the core flow of the shadowgraph are at similar angles. These large differences could easily be attributed to the modeling of the flow in 2-D rather than axisymmetric or 3-D. The 2-D effects seem to have a more pronounced affect at the higher pressure ratios of the main propellant flow.

In Figure 15 at $t_{\text{exp}} = +60 \mu\text{s}$, the main propellant flow had developed. The distortion of the front blast wave can be seen more readily in the DG results.

This is most likely a result of mixing effects and turbulence in the main propellant flow. The rear blast wave from the main propellant flow is not as perpendicular to the barrel as the results as the precursor blast wave. This could be the result of the precursor and main blast wave interaction not being modeled properly in addition to errors in the boundary conditions.

In Figure 16 at $t_{\text{exp}} = +120 \mu\text{s}$, the bullet is clearly visible in the shadowgraph image. The bullet movement was not modeled in the DG results. The free-shear layer and barrel shock now show a much higher angle for the DG results than for the shadowgraph results. In addition, the forward shape of the blast wave is now more distorted with the DG results. The back edge of the blast wave cannot be seen in the shadowgraph image, but is shown in the DG results. This indicates that this wave propagation is being retarded for some reason.

In Figures 17 and 18 are shown pressure vs. distance along the 135-degree radial line emanating from the muzzle at $t_{\text{exp}} \approx -350 \mu\text{s}$ and $t_{\text{exp}} \approx -250 \mu\text{s}$ for both the Fluent and DG results. The peak pressure (referred to as peak overpressure in blast terminology) and distance from the muzzle blast wave are similar for both the Fluent and DG results indicating similar time accuracy and ability to maintain shock strength at these flow times. The DG results show a sharper shock front than the Fluent results however. This becomes very important as flow solution time increases. Once this shock becomes less and less sharp, the peak overpressure starts to drop and the wave begins to dissipate. The DG results also show more noise on the rear side of the blast

wave. This is a result of the disturbances that are propagating into the flow field being resolved by DG and not by Fluent. Also, for $t_{\text{exp}} \approx -250 \mu\text{s}$, Fluent is predicting the wave front being farther from the muzzle than DG, but with a similar shape. DG shows a negative pressure in front of the blast wave that Fluent does not. Both codes model the negative pressure drop behind the blast wave.

In Table 1 is shown a comparison between the shadowgraph and DG of the distance from the muzzle centerline to the forward edge and rear edge along the barrel of the blast wave. This is done in order to compare the time accuracy of DG to the experimental results. As can be seen, the forward blast wave propagates about 22% faster than the experimental results for DG when looking at the -250 and $-80 \mu\text{s}$ times. This could indicate a problem with the boundary conditions as well as time accuracy of the code. When looking at Figure 18, the rear blast wave for Fluent is moving even faster than DG. This seems to indicate time accuracy with blast wave modeling may be difficult, especially if initial conditions are incorrect.

Computation Comparison

DG and Fluent are compared to each other as well as different levels of refinement. Comparison simulations were run on a 2.4 GHz Xeon Dual Processor Dell Precision 530 with 1.0 GB of memory running Linux. In each case, a single processor was utilized to perform a serial computation. Grid sizes and computation times are compared as well as overall results.

Shown in Figure 19 is a comparison of DG and Fluent at 2-levels and 4-levels of refinement at $t_{\text{exp}} \approx -350 \mu\text{s}$. Computation times and final grid sizes are shown below each logarithmic density contour. In addition, the grid structure is overlaid on the contour plot for each result. All flow equation computations are inviscid calculations with first-order equations. The same initial quad-paved grid is utilized for all computations. Grid adaption in both cases was performed on density

For the 2-level adaption case, Fluent and DG have similar computation times, however Fluent utilizes about twice as many elements as DG. In addition, the shock structure is sharper with DG than with Fluent. For the 4-level adaption case, Fluent utilizes an order of magnitude more elements than DG and almost twice the computation time.

It would appear that Fluent is about five times faster per element than DG for the 4-level case where Fluent takes twice as long to perform calculations on about ten times as many grid elements. However, DG used far fewer cells than Fluent and half the computation time to produce better results for the 4-level case. This would indicate that DG could produce better results with fewer grid elements than Fluent.

Some of the difference in computation time between DG and Fluent can be attributed to the fact that DG is a research level code that has not been optimized. However, one would expect there to be more computational overhead with a discontinuous calculation like DG as compared to a standard solver like Fluent.

When comparing the results, DG is capable of maintaining shock sharpness, regardless of refinement level. Even with a 2-level grid adaption, the outer blast wave is just as sharp with the 2-level grid as with the 4-level grid. When comparing Fluent 2-level and 4-level grid adaption, the shock structure is markedly smeared with the 2-level adaption. This would seem to indicate that standard solvers such as Fluent require high levels of grid adaption to maintain shock strength in moving shock and blast problems. Discontinuous solvers such as DG do not require refining to maintain shock strength. This is a huge advantage of discontinuous solvers. One can get reasonable results even with rather coarse grids, thereby making simulations that are more difficult feasible. This is the case for full 3-D problems where one is trying to determine shock strength at long distances from the gun muzzle.

Conclusions

Several conclusions can be drawn from this study of CFD application to gun muzzle blast. These include:

- 1) The 7.62 mm NATO G3 CFD precursor flow results matched shadowgraph results well, however, the main propellant flow did not match as well.
- 2) Unsteady grid adaption (h-adaptivity) is a critical technology to modeling gun muzzle blast.
- 3) It is possible to get good results from standard solvers with high levels of adaption.
- 4) Discontinuous solvers can model blast with coarser grid adaption than standard solvers.
- 5) Discontinuous solvers can model blast better than standard solvers for a given level of refinement.
- 6) Discontinuous solvers can potentially require longer solution time than standard solvers.
- 7) Modeling blast waves utilizing 2-D grids. It is recommended that axisymmetric or 3-D grids be used when possible.

Acknowledgments

Special thanks goes to Thomas Gessner and Christoph Hiemke from Fluent for assisting with the development of Fluent 6.1.11 and for providing solutions for the 7.62 mm problem.

All CFD results presented in this paper were created using EnSight produced by CEI.

Mention of products or software in this paper in no way constitutes endorsement by the government of any of its parties.

References

1. Klingenberg, Gunter; Heimerl, Joseph M.; Seebass, A. Richard Editor-in-Chief. Gun Muzzle Blast and Flash, Progress in Astronautics and Aeronautics, Vol. 139; AIAA, Washington, DC 1992.
2. Dillon, Robert. "A Method of Estimating Blast Envelope Duration", Proceedings of the Ninth U.S. Army Symposium on Gun Dynamics, U.S. Army Armament Research and Development and Engineering Center, McLean, Virginia, November 17-19, 1998.
3. Klingenberg, Gunter; Heimerl, Joseph M.; Seebass, A. Richard

Editor-in-Chief. Originally published in Gun Muzzle Blast and Flash, Progress in Astronautics and Aeronautics, Vol. 139; AIAA, Washington, DC 1992 Copyright © 1992 by the American Institute of Aeronautics and Astronautics, Inc. Reprinted with permission.

4. Carofano, Garry C. "Blast Computation Using Harten's Total Variation Diminishing Scheme", ARLCB-TR-84029, US Army Armament Research & Development Center, Benet Weapons Laboratory, SMCAR-LCB-TL, Watervliet, NY 12189.
5. Remale, J.F.; Flaherty, J.E.; Shephard, M.S. "An Adaptive Discontinuous Galerkin Technique with an Orthogonal Basis Applied to Compressible Flow Problems." SIAM Journal on Scientific Computing, 2002.
6. Reed, W. & Hill, T. "Triangular mesh methods for the neutron transport equation", Tech. Report LA-UR-73-479, Los Alamos Scientific Laboratory, 1973.

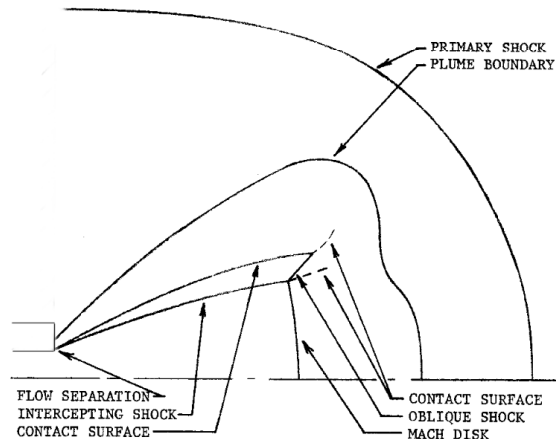


Figure 1. Muzzle flow characteristics (Taken from reference 4).

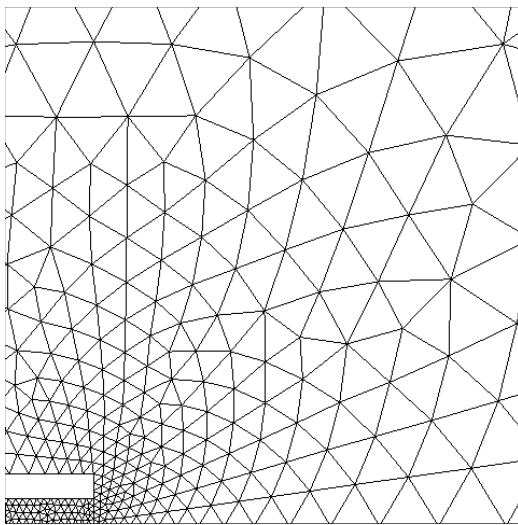


Figure 2. Initial tri-grid

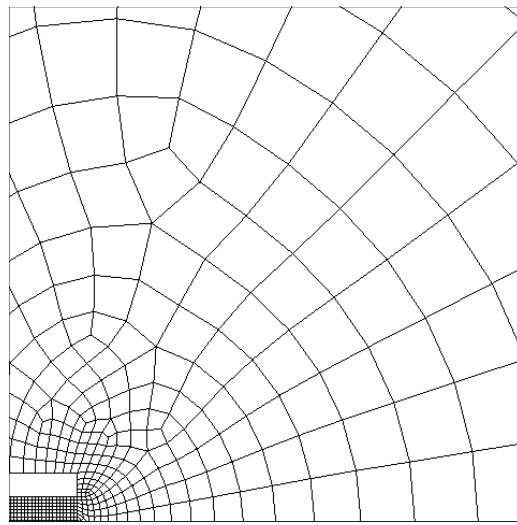


Figure 3. Initial quad-grid

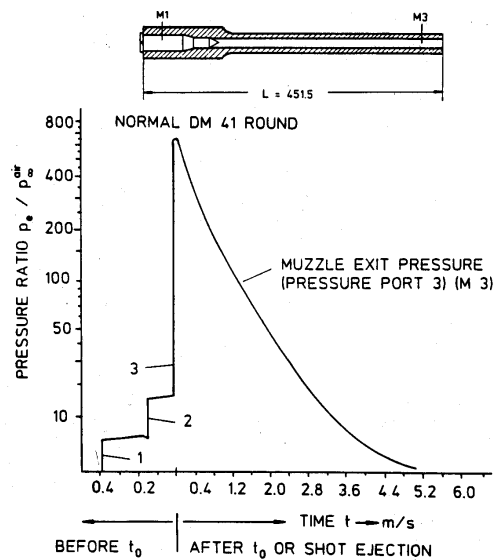


Figure 4. Figure 6.24 taken from reference 3 showing gun geometry and pressure ratio profile for position M3.

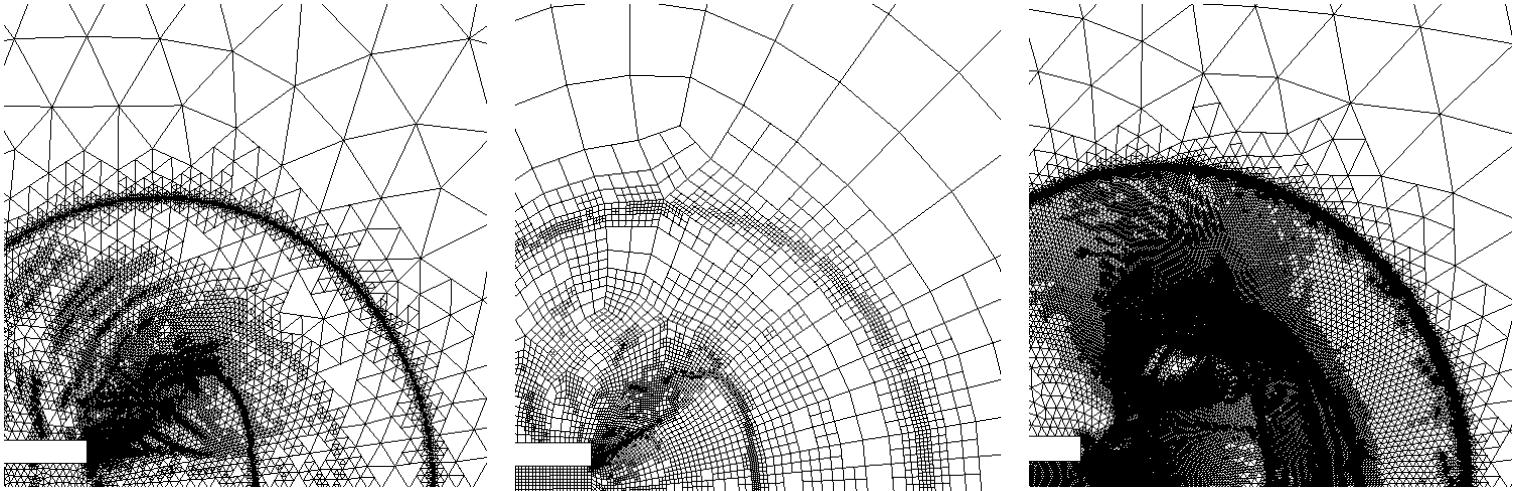


Figure 5. Unstructured non-conformal DG 5-level tri-grid (left), DG 4-level quad-grid (middle), and $2.5 \times 10^{-8} \text{ m}^2$ minimum cell size Fluent tri-grid at $t \approx 1.0 \times 10^{-4} \text{ sec}$.

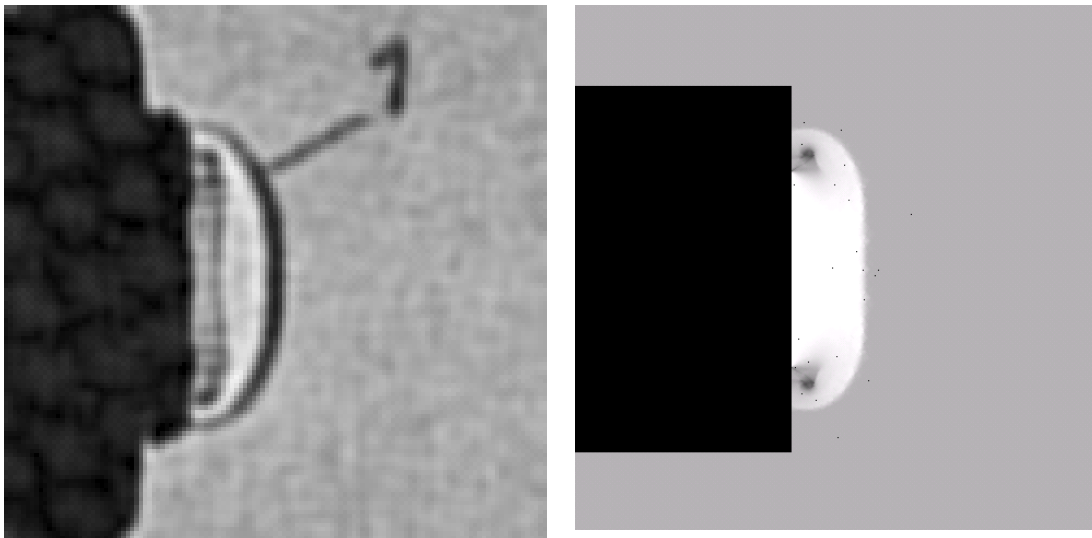


Figure 6. Shadowgraph³ (left) and DG 5-Level tri-grid adaption logarithmic density contour (right) at $t_{\text{exp}} = -395 \mu\text{s}$.

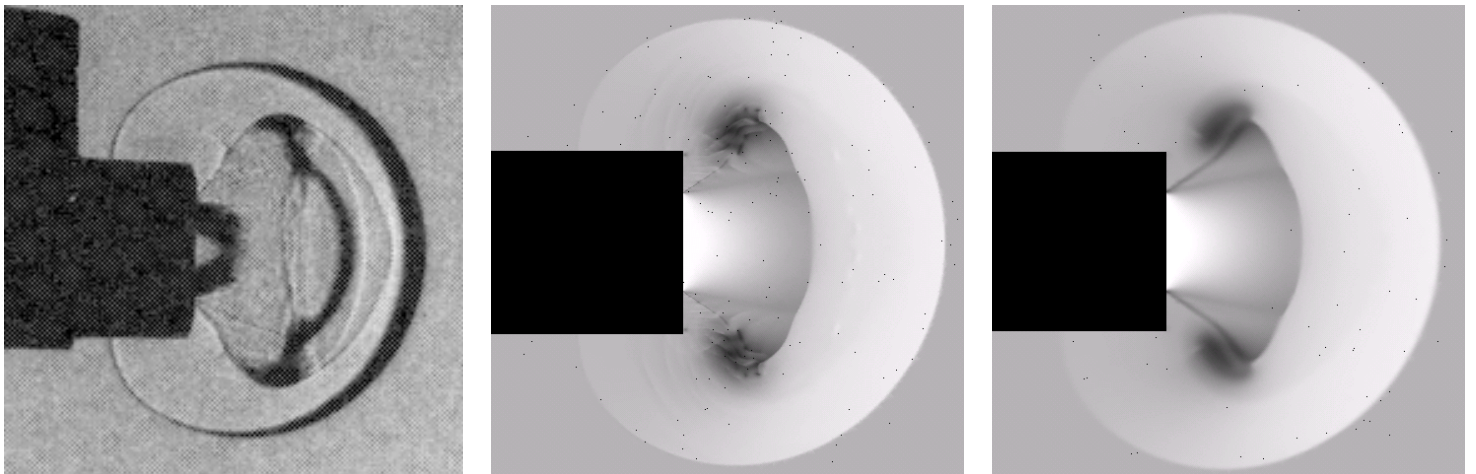


Figure 7. Shadowgraph³ (left), DG 5-Level adaption logarithmic density contour (middle), and Fluent $2.5 \times 10^{-8} \text{ m}^2$ cell volume limit adaption at $t_{\text{exp}} \approx -370 \mu\text{s}$.

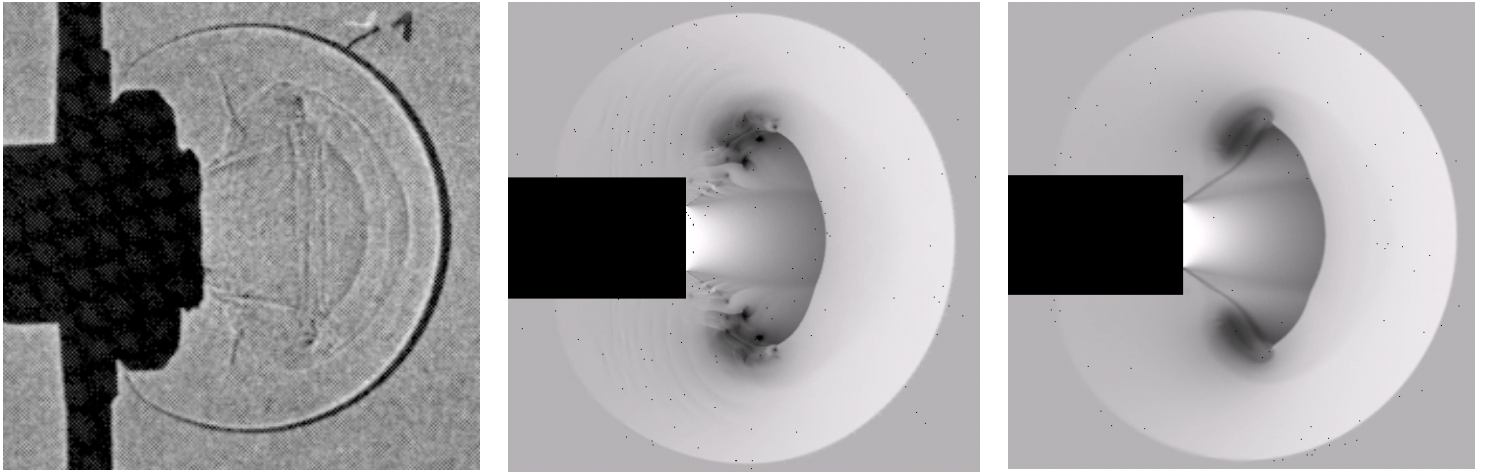


Figure 8. Shadowgraph³ (left), DG 5-Level adaption logarithmic density contour (middle), and Fluent 2.5e-8 m² cell volume limit adaption at $t_{exp} \approx -350 \mu s$.

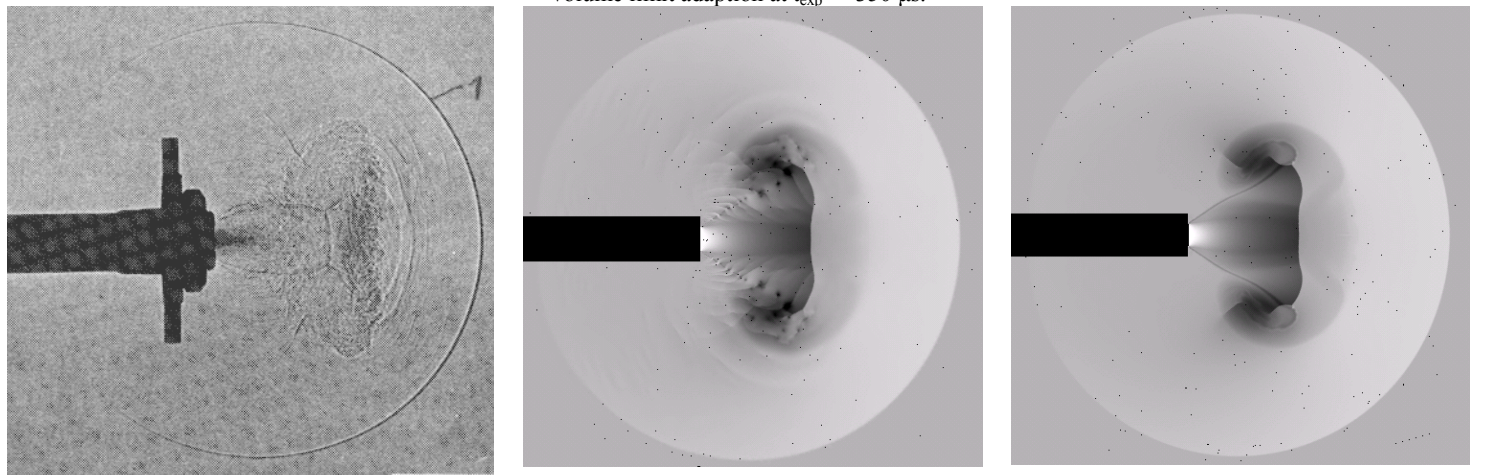


Figure 9. Shadowgraph³ (left), DG 5-Level adaption logarithmic density contour (middle), and Fluent 2.5e-8 m² cell volume limit adaption at $t_{exp} \approx -250 \mu s$.

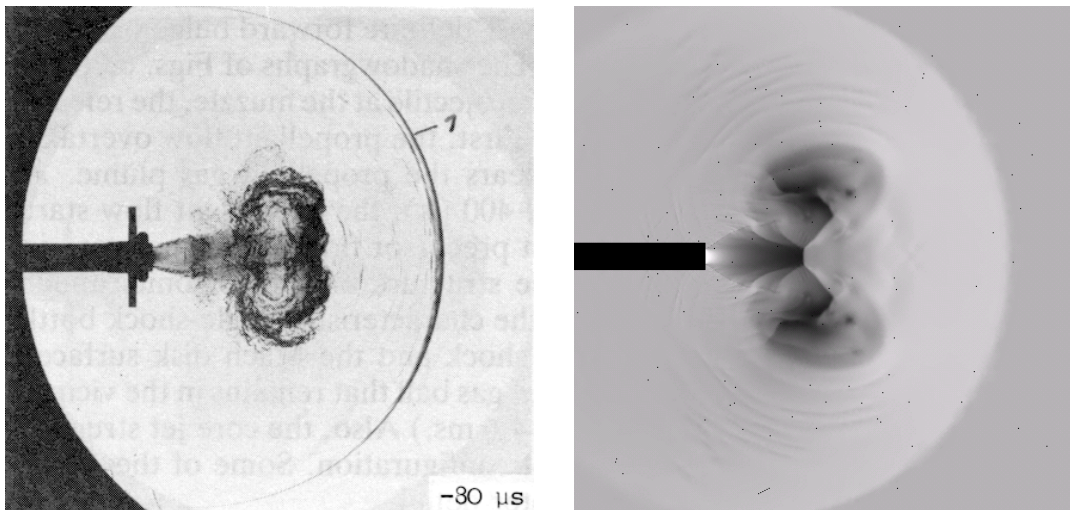


Figure 10. Shadowgraph³ (left) and DG 4-Level adaption logarithmic density contour (right) at $t_{exp} = -80 \mu s$.

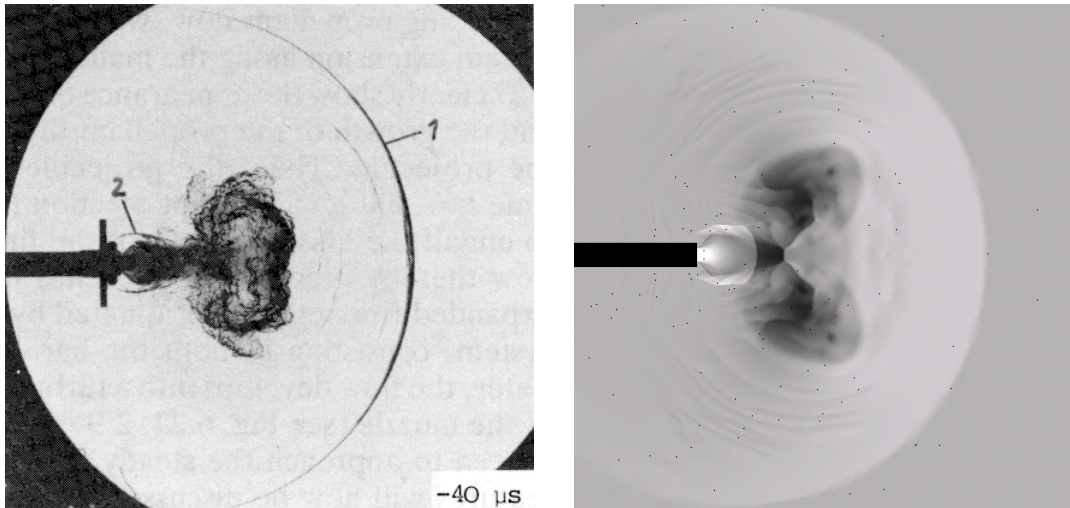


Figure 11. Shadowgraph³ (left) and DG 4-Level quad-grid adaption logarithmic density contour (right) at $t_{\text{exp}} = -40 \mu\text{s}$.

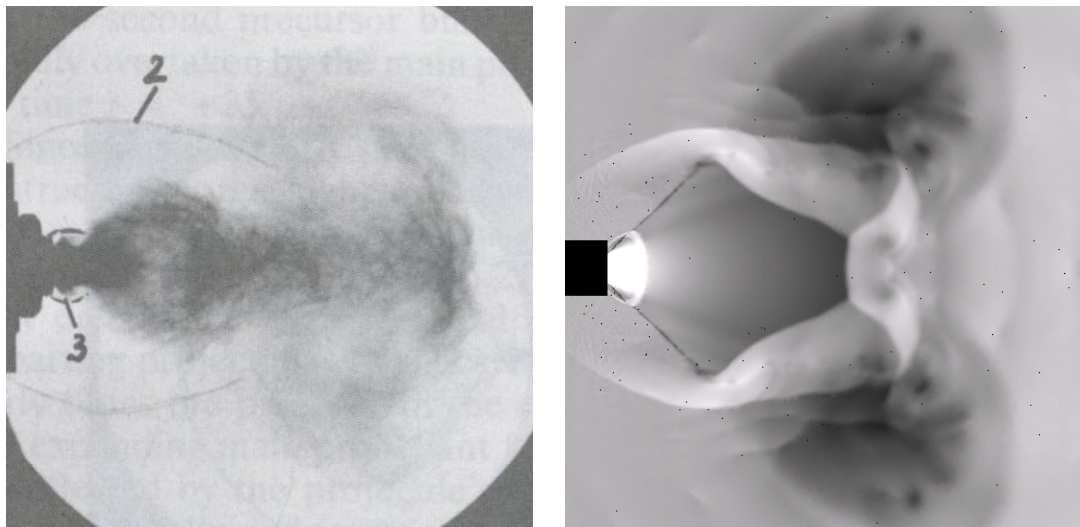


Figure 12 Shadowgraph³ (left) and DG 4-Level quad-grid adaption logarithmic density contour (right) at $t_{\text{exp}} = -5 \mu\text{s}$.

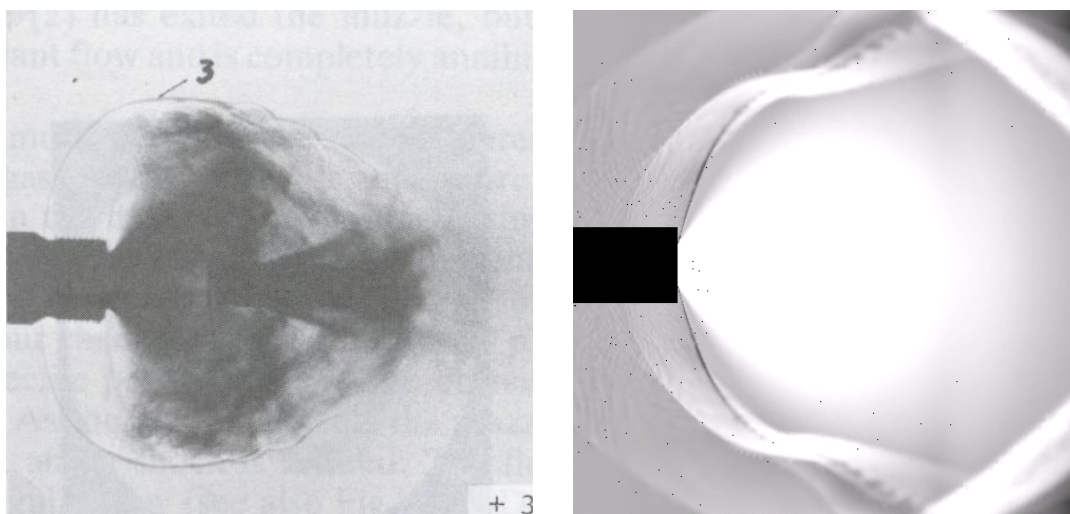


Figure 13. Shadowgraph³ (left) and DG 4-Level quad-grid adaption logarithmic density contour (right) at $t_{\text{exp}} = +35 \mu\text{s}$.

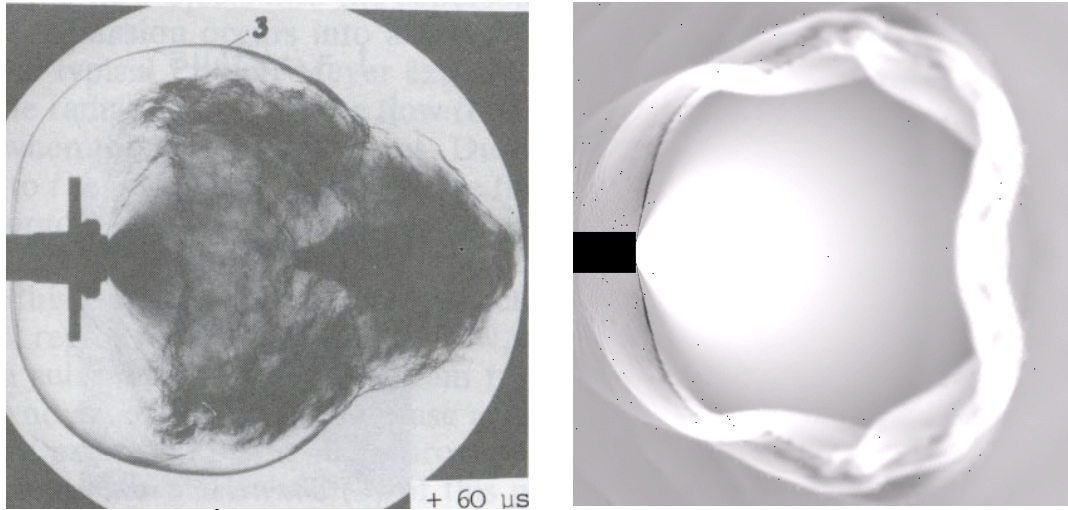


Figure 15. Shadowgraph³ (left) and DG 4-Level quad-grid adaption logarithmic density contour (right) at $t_{\text{exp}} = +60 \mu\text{s}$.

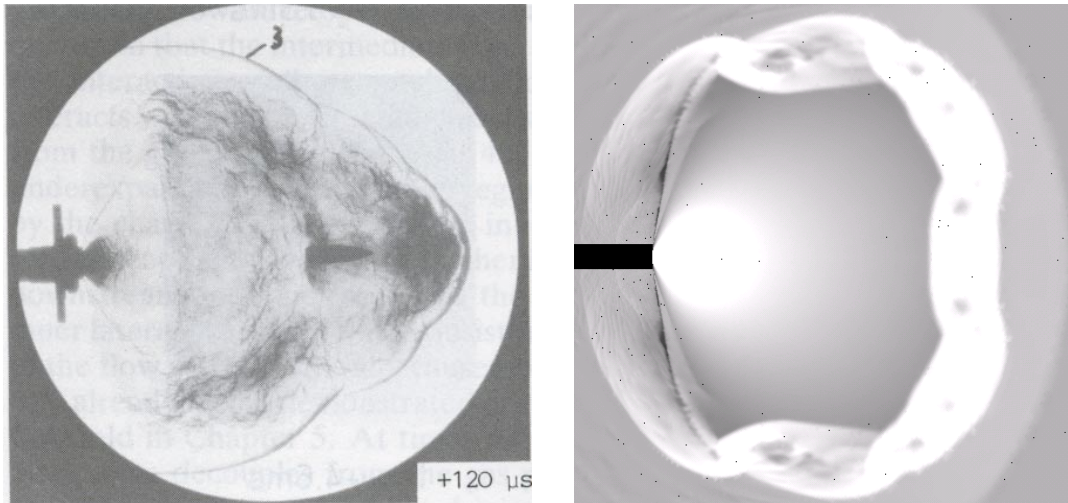


Figure 16. Shadowgraph³ (left) and DG 4-Level quad-grid adaption logarithmic density contour (right) at $t_{\text{exp}} = +120 \mu\text{s}$.

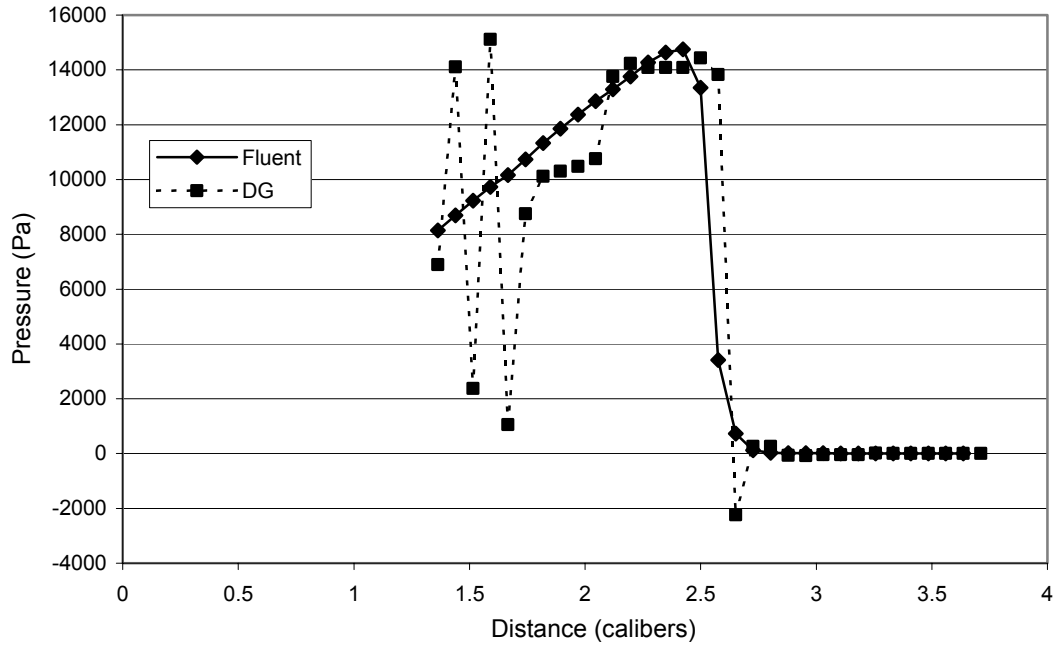


Figure 17. Comparison of Fluent and DG pressure vs. distance along the 135 degree radial at $t_{exp} \approx -350 \mu s$. The 0 degree radial is the direction of fire and the center of rotation is at the muzzle.

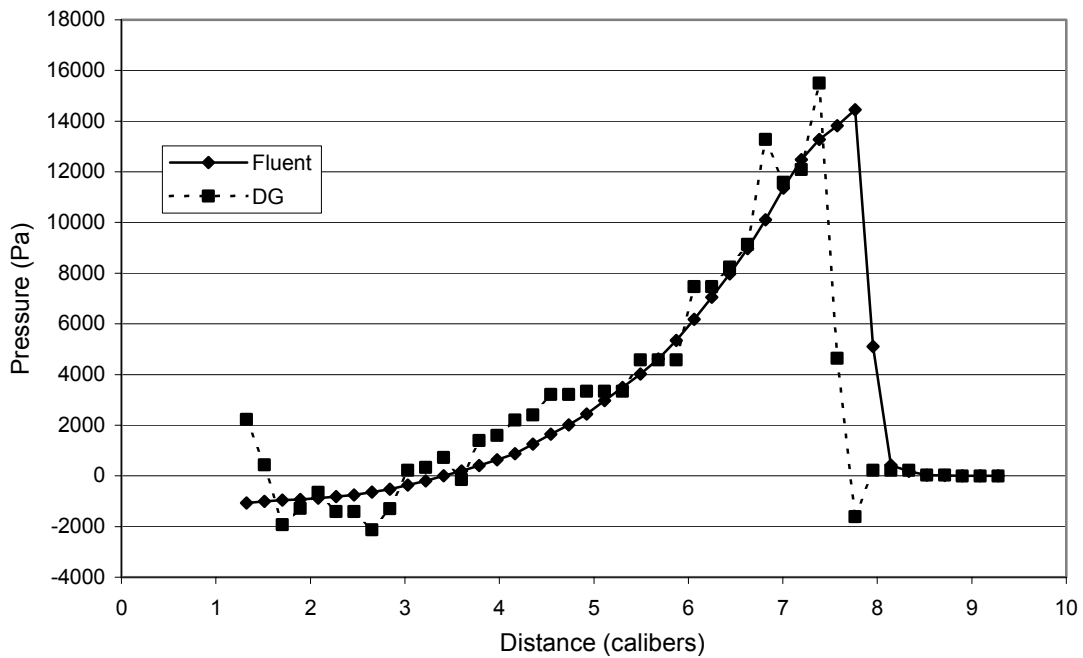


Figure 18. . Comparison of Fluent and DG pressure vs. distance along the 135 degree radial at $t_{exp} \approx -250 \mu s$. The 0 degree radial is the direction of fire and the center of rotation is at the muzzle.

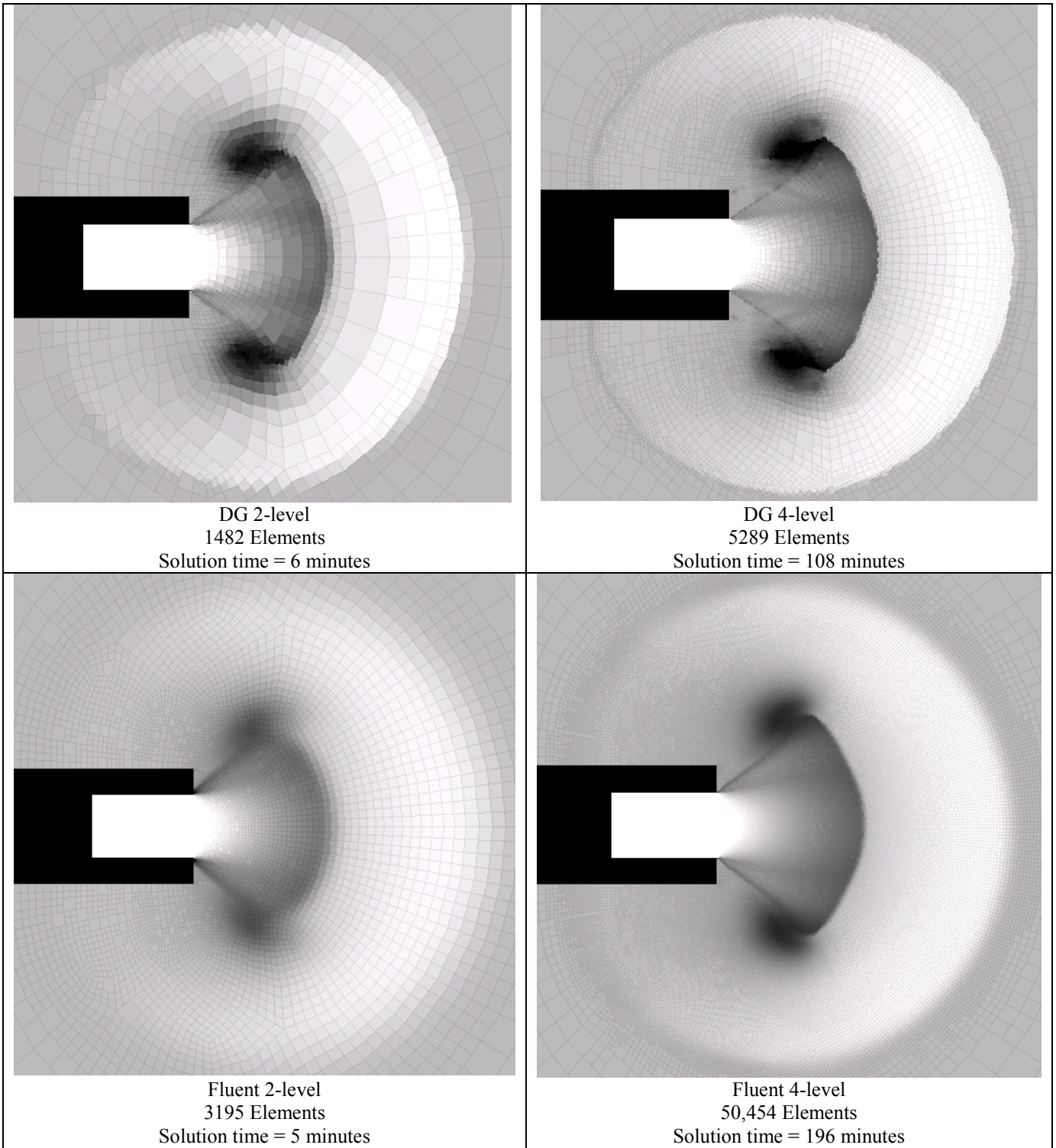


Figure 19. Adaption level and solution time comparison of DG quad-grid and Fluent quad-grid. DG 2-level (top left) and 4-level (top right) and Fluent 2-level (bottom left) and 6-level (bottom right). Results are at $t_{exp} \approx -350 \mu s$.

t_{exp}	Distance Rear (along barrel) CFD, cal	Distance Rear (along barrel) Shadowgraph, cal	Distance Front CFD, cal	Distance Front Shadowgraph (cal)
-395 μ s	N/A	N/A	0.4	0.5
-350 μ s	2.2	2.1	4.2	3.0
-250 μ s	6.8	Not visible	10.7	8.7
-80 μ s	14.7	Not visible	20.7	16.9

Table 1. First precursor blast wave distance comparison.